Evaluating indent pile-up with metallic films on ceramic-like substrates

MariAnne Sullivan and Barton C. Prorok[a)]
Department of Mechanical Engineering, Auburn University, Auburn, Alabama 36849, USA

(Received 6 January 2015; accepted 27 May 2015)

This work focused on ascertaining the effect of pile-up during indentation of thin films on substrates. Conventional understanding has postulated that differences in contact area resulting from pile-up or sink-in significantly alter the extraction of material properties. In this work, the specific case of pile-up with compliant, plastically deforming films on stiff, nonplastically deforming substrates was studied. Several literature methods to assess pile-up were leveraged, and a new technique was developed and validated to quantify projected pile-up. Indentation testing was performed on gold films of multiple thicknesses on several ceramic-based substrates. The results indicated that the degree of pile-up was solely a function of indent depth into the film. Pile-up was not influenced by film thickness or substrate elastic modulus. In other words, the pile-up development was insensitive to the presence of the substrate and how it contributes to the composite's elastic properties. In such case, if the elastic response of the film/substrate composite was independent of the degree of pile-up, then elastic data acquired from unloading did not require a contact area correction. The findings are confirmed using the Zhou–Prorok model for extracting film elastic properties for both gold and platinum films.

I. INTRODUCTION

In the past several decades, the mechanical properties of thin films have been an important aspect in applications, such as electronics, protective coatings, and microelectrical mechanical systems. Nanoindentation has become a popular tool to evaluate these properties of thin film materials because it is minimally destructive and there is no need to image the indent.[1–9] Various models have been developed to account for substrate effects, including Doerner and Nix[4] with modifications,[5,6] Gao et al.,[7] and more recently from Zhou and Prorok.[10,11] In addition, there have been barriers to collecting accurate values due to pile-up and sink-in during nanoindentation.[12]

Generally in film/substrate systems, pile-up occurs when there is a compliant film on a stiff substrate, and sink-in when there is a stiff film on a compliant substrate,[13] leading to a difference in the indent impression, see Fig. 1. A normal indent from a Berkovich indenter tip is presented in Fig. 1(a), followed by (b) pile-up, and (c) sink-in. These are represented by platinum films on (a) platinum, (b) silicon oxide, and (c) tin. Previous researchers have shown that pile-up and sink-in can affect the contact area of the indenter, which in turn can alter the extracted mechanical properties.[14,15] An indent experiencing pile-up underestimates contact area because area due to the additional pile-up is not included. Inversely, sink-in produces an overestimation of contact area.[6,14–16]

These phenomena can play a role in the calculations of extracting film properties when using the Oliver–Pharr method.[1] Here, a reduced modulus is found that eliminates deformation of the indenter tip itself via: $1/E_r = (1-\nu^2)/E + \left(1-\nu_i^2\right)/E_i$ where E and ν are elastic modulus and Poisson's ratio relating to the material, and E_i and ν_i pertain to the indenter properties.[1] This reduced modulus is then related to the unloading stiffness via Eq. (1).

$$S = \frac{dP}{dh} = \beta \frac{2}{\sqrt{\pi}} E_r \sqrt{A} \quad , \tag{1}$$

where S is the stiffness, defined by dP/dh, P being the load, h the displacement, and β a geometrical term, close to 1 for a Berkovich tip.[1] Here, A is the projected contact area from Berkovich tip geometry based upon indent depth. Typically, this variable is not adjusted when contact area changes under pile-up or sink-in conditions.

The Zhou–Prorok model was chosen as an analysis technique because it appears to be adept at describing the elastic behavior of many different film and substrate combinations.[10,11] Eq. (2) is the Zhou–Prorok model which has a basic form of the inverse rule of mixtures with weighting factors that describe the interplay between film and substrate:

$$\frac{1}{E'} = \frac{1}{E_f'}(1-\Phi_s) \cdot \left(\frac{E_f'}{E_s'}\right)^{0.1} + \frac{1}{E_s'}\Phi_f \quad . \tag{2}$$

Contributing Editor: George M. Pharr
[a)]Address all correspondence to this author.
e-mail: prorobc@auburn.edu
DOI: 10.1557/jmr.2015.167

 © Materials Research Society 2015

https://doi.org/10.1557/jmr.2015.167 Published online by Cambridge University Press

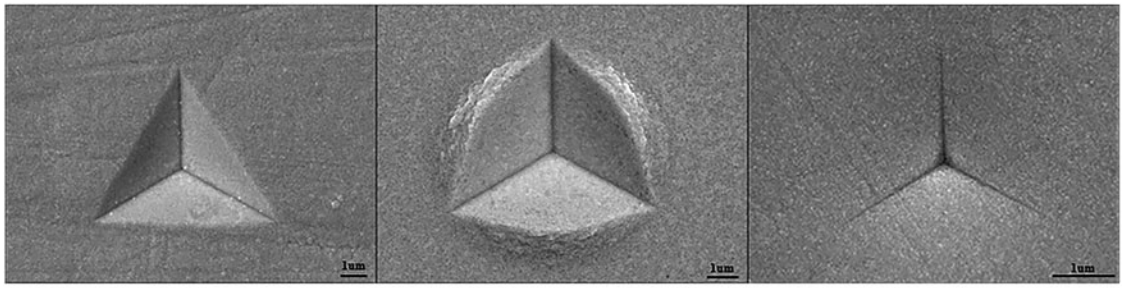


FIG. 1. (a) Normal indent impression with Berkovich tip, (b) indent with pile-up, and (c) indent with sink-in.

Here, E' is the composite or reduced modulus from the indenter, E_f' is the film modulus, E_s' is the substrate modulus, the weighting factors $\Phi_f = e^{-\nu_f(t/h)}$ and $\Phi_s = e^{-\nu_s(t/h)}$ where υ_f and υ_s are film and substrate Poisson's ratios, respectively, t is the thickness of the film, and h is the displacement into the film. A comparison of this model with other models is seen in prior work.[10,11] In this work, the described model was leveraged to assess how additional contact area due to pile-up affects elastic properties.

II. EXPERIMENTAL PROCEDURE

A. Materials selection

In this work, the authors chose to study how pile-up affects the extraction of elastic properties of the film/substrate composite by selecting a series of materials that consisted of compliant films on stiff substrates. Gold was an ideal choice for the film material due to its low modulus, capacity for plastic deformation, ease of deposition, and inertness. Substrate materials included single crystal forms of silicon (Si), aluminum oxide (Al_2O_3), aluminum nitride (AlN), and magnesium oxide (MgO). Negligibly plastically deforming substrates, termed non-plastically deforming in this work, were chosen to avoid accounting for plastic deformation in the substrate during the analysis.[16] The elastic modulus from indenting bulk samples as well as literature values of Poisson's ratios of these materials are given in Table I.

TABLE I. Material properties from experimental and literature values.

Material	Elastic modulus, E (GPa)	Poisson's ratio, ν
Au	76 ± 5	0.42 (Ref. 17)
Pt	168 (Ref. 17)	0.39 (Ref. 17)
Si	179 ± 3	0.28 (Ref. 17)
Al_2O_3	350 ± 8	0.22 (Ref. 17)
AlN	302 ± 14	0.26 (Ref. 18)
MgO	345 ± 7	0.23 (Ref. 19)

TABLE II. Sputter coating conditions.

Presputter power	100 W
Presputter time	60 s
Sputter power	100 W
Gas (Ar) flow	25 sccm

B. Film deposition

Gold films were simultaneously deposited on all four substrates using a Denton Discovery 18 sputtering system under DC power and substrate rotation. Conditions were chosen from previous work on sputtering gold films.[10,11,20–22] The resulting microstructure is typically columnar with a (111) texture.[23] A titanium layer 10 nm thick was sputtered beforehand to promote adhesion. Table II lists the physical parameters used with film thickness being controlled by sputter time. Three film thicknesses were used (360, 625, and 950 nm) to ascertain the role that film thickness may play during film pile-up. Film thickness was measured in multiple locations with a Bruker/Veeco Dektak 150 Profilometer (Billerica, MA).

C. Testing and evaluating

Nanoindentation was performed using an MTS Nanoindenter XP with a Berkovich diamond tip under continuous stiffness operation with a harmonic displacement target set at 2 nm and a minimum thermal drift rate of 0.05 nm/s. The samples were indented to various depths and the values of elastic modulus were continually recorded throughout displacement. Arrays of at least twenty five indents with 50 micrometer spacing were performed for each experimental condition to obtain a statistical response. Residual indents were imaged with a JEOL JSM 7000F scanning electron microscope (SEM; Tokyo, Japan). ImageJ software[24] was used to accurately measure the projected indenter area and projected pile-up area. These measurements were recorded and compared among all film/substrate combinations at varying depths.

III. RESULTS AND DISCUSSION

Plots of the measured composite modulus versus displacement into the surface obtained from indenting three

https://doi.org/10.1557/jmr.2015.167 Published online by Cambridge University Press

gold films 360, 625, and 950 nm thick on a silicon substrate are shown in Fig. 2(a). This plot shows the average values of measured modulus for 25 indents in each film thickness denoted by: 360 nm (▲), 625 nm (●), and 950 nm (■). The error bars illustrate the standard deviation at each indentation depth. It should be noted that this analysis was confined to metallic films under 1 micrometer thick. As film thickness increases beyond this, grain size and microstructure evolve, altering the yield stress of the material and consequently the degree of pile-up.

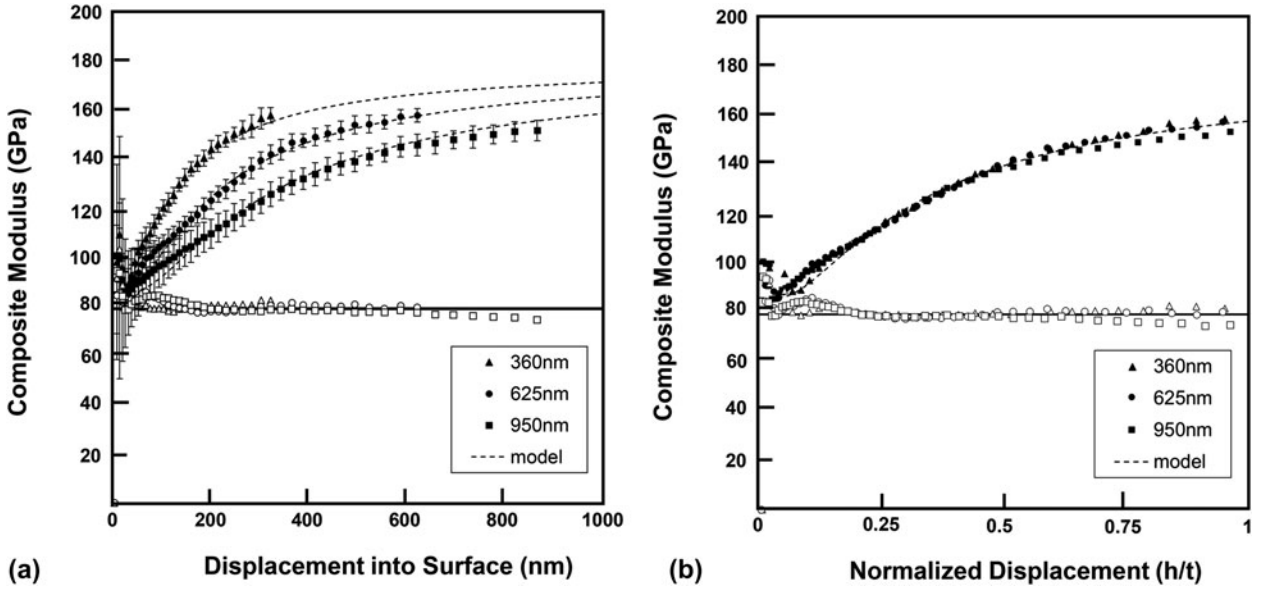


FIG. 2. (a) Experimental values of modulus versus displacement for the three gold films deposited on a silicon substrate (closed markers), the Zhou–Prorok model prediction (dashed lines), and extracted film modulus (open markers). (b) Experimental data collapsed onto a single line using the normalized displacement, i.e., removing thickness dependence.

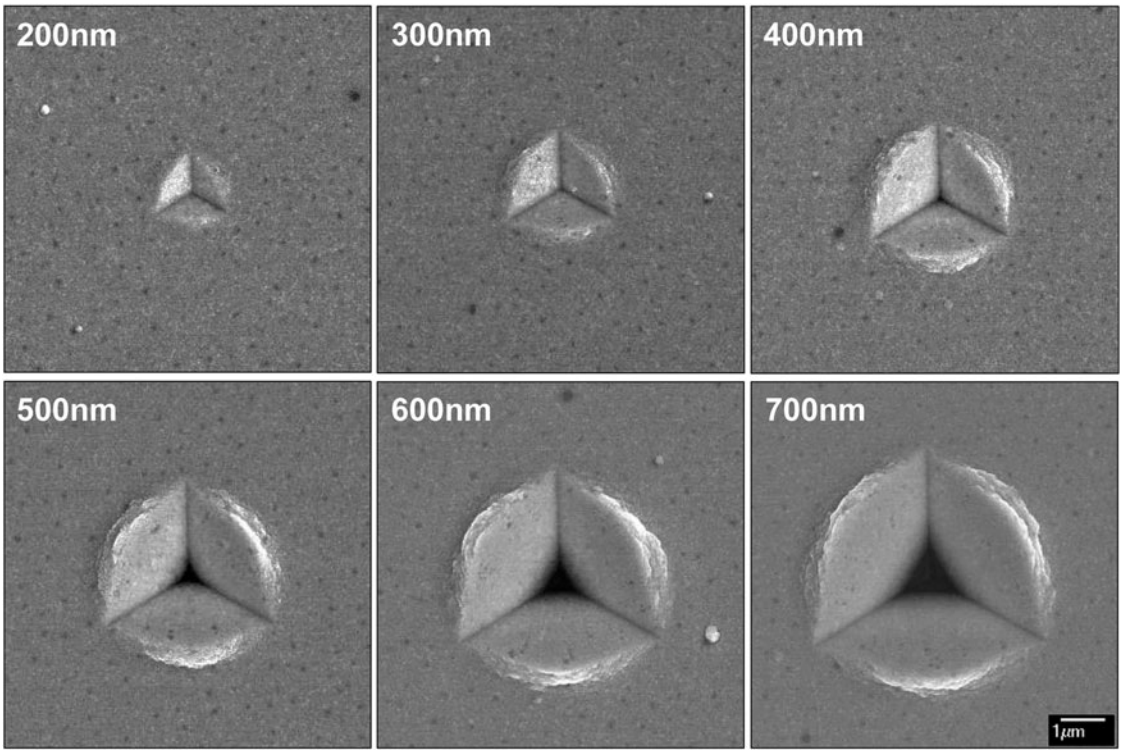


FIG. 3. Indent impression progression of 360 nm gold film on silicon from 200 to 700 nm.

https://doi.org/10.1557/jmr.2015.167 Published online by Cambridge University Press

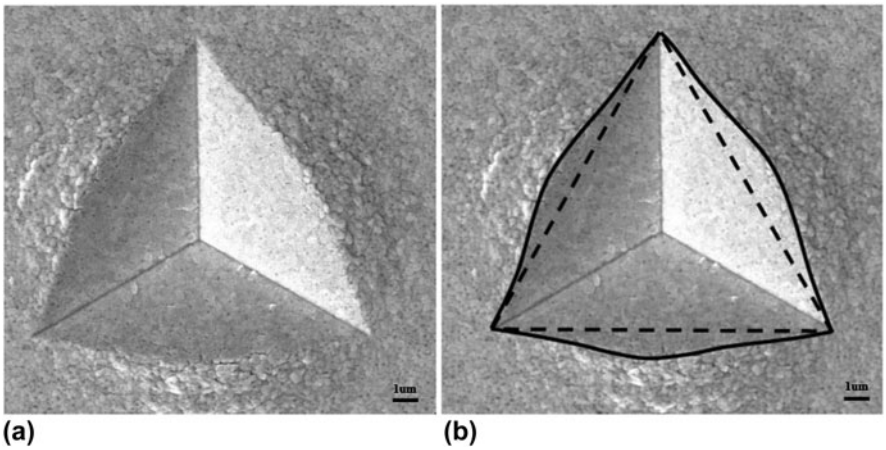


FIG. 4. (a) Indent impression with pile-up, (b) dotted lines depicting Berkovich projected area, solid lines for total area. Subtracting projected area total area results in pile-up area.

Each set of data was truncated at the point where the indent depth equaled the film thickness, or when the indenter penetrated to the substrate. The thinner films exhibited a stiffer composite response, as at any given displacement, more of the stiffer substrate would have been engaged. The Zhou–Prorok model described in Eq. (2) was applied to this plot using the material property values listed Table I, represented by the dashed lines. The agreement between the model and experiments indicated that one could extract film elastic modulus from the experimental data using bulk literature values of the other parameters. These extracted film modulus values are designated by open symbols for 360 nm (△), 625 nm (○), and 950 nm (□). Results from each film thickness fall on a single consistent line of approximately 79 GPa, which agree well with experimental literature values using alternate techniques (solid line).[20–22,25–28]

To better illustrate how the Zhou–Prorok model describes these three composites, the composite modulus was plotted as a function of normalized displacement, (h/t), in Fig. 2(b). In other words, the effect of film thickness was removed. In this representation, all the experimental results and model predictions from the three film thicknesses converged onto a single curve. The extracted film modulus remained consistently around 79 GPa, regardless of film thickness or penetration depth.

One can question, then, how this model performs so well when considering that varying degrees of pile-up must exist for different film thicknesses and penetration depths. Figure 3 is a compilation of scanning electron micrographs illustrating the residual indent and its associated pile-up as the indenter penetrates the film. These images are from the 360 nm thick gold film on a silicon substrate at penetration depths of 200 through 700 nm. As the indenter penetrated the film, the degree of pile-up significantly increased. At 400 nm depth and deeper, the silicon substrate can be seen as the dark

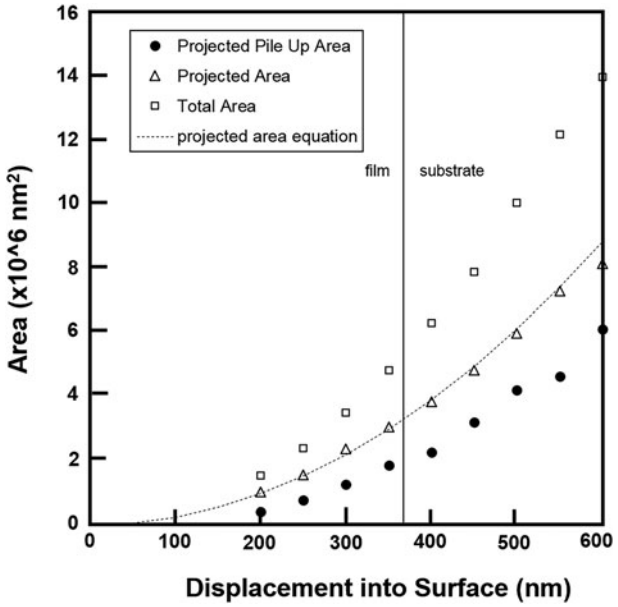


FIG. 5. Projected pile-up area (●), projected area (△), and total area (□) for 360 nm gold film on silicon, where the projected area follows the equation for the Berkovich tip.

region in the center of the indent where the indenter has punched through the film. It is curious to note that the Zhou–Prorok model applied here appeared to accurately predict the elastic behavior of the composite even though the film experienced an increasing degree of material pile-up with indent penetration. Furthermore, when the film modulus was extracted, it did not appear to be influenced by this increased degree of pile-up. It has been generally accepted in the indentation community that when this pile-up is not accounted for, the indenter should overestimate the composite modulus.[6,14–16] This arises as the Oliver–Pharr method models indenter contact as a function of Berkovich contact area via $A = 24.5h_c^2$.[1,2] The method

https://doi.org/10.1557/jmr.2015.167 Published online by Cambridge University Press

was used to obtain the composite modulus values shown in Fig. 2. These were all calculated from the unloading stiffness using Eq. (1) with no correction or consideration of additional pile-up area. It appears that the applied

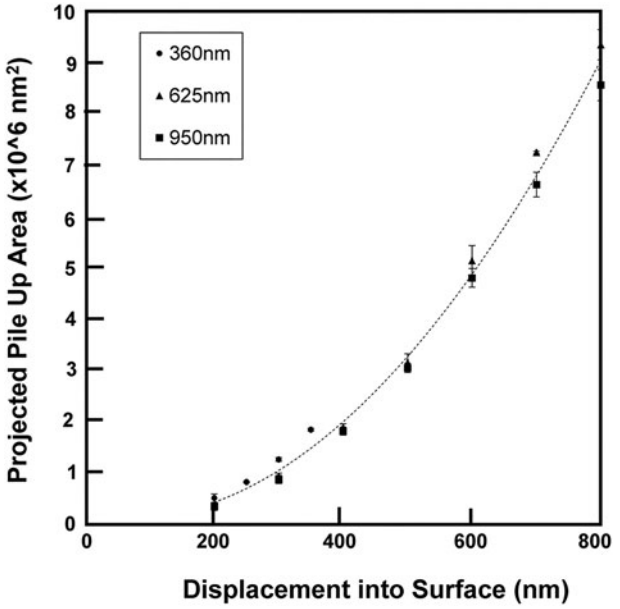


FIG. 6. Pile-up area for three thicknesses of gold on silicon, all following the same trend with increasing displacement into surface.

Zhou–Prorok model either accounted for the influence of the additional pile-up area or the additional area played no role in the elastic property extraction. In examining the construct of the model [Eq. (2)] there appears to be no variables that are physically connected to any aspect of projected contact area, be it from the indenter tip or pile-up. The only time a projected area played a role in determining the data in Fig. 2 was through the Oliver–Pharr use of Eq. (1). Thus, it appears more likely that the extra contact from pile-up may not have contributed to the measured elastic response during indent unloading.

To assess whether or not pile-up played a role in elastic modulus calculations, a method to directly measure and quantify the degree of additional projected contact area from pile-up was developed. Here, the authors sought a method that enabled the additional contact area to be calculated from two-dimensional electron micrographs, mainly to reduce tedious atomic force microscopy (AFM) measurements. Of the many techniques described in the literature,[29–32] the method developed by Kese et al. best fit this role. A semi-ellipse shape was used to measure and predict pile-up area by roughly fitting geometric shapes to the piled-up area. The authors adapted insight in this work into a simpler method using only the two-dimensional electron micrograph and

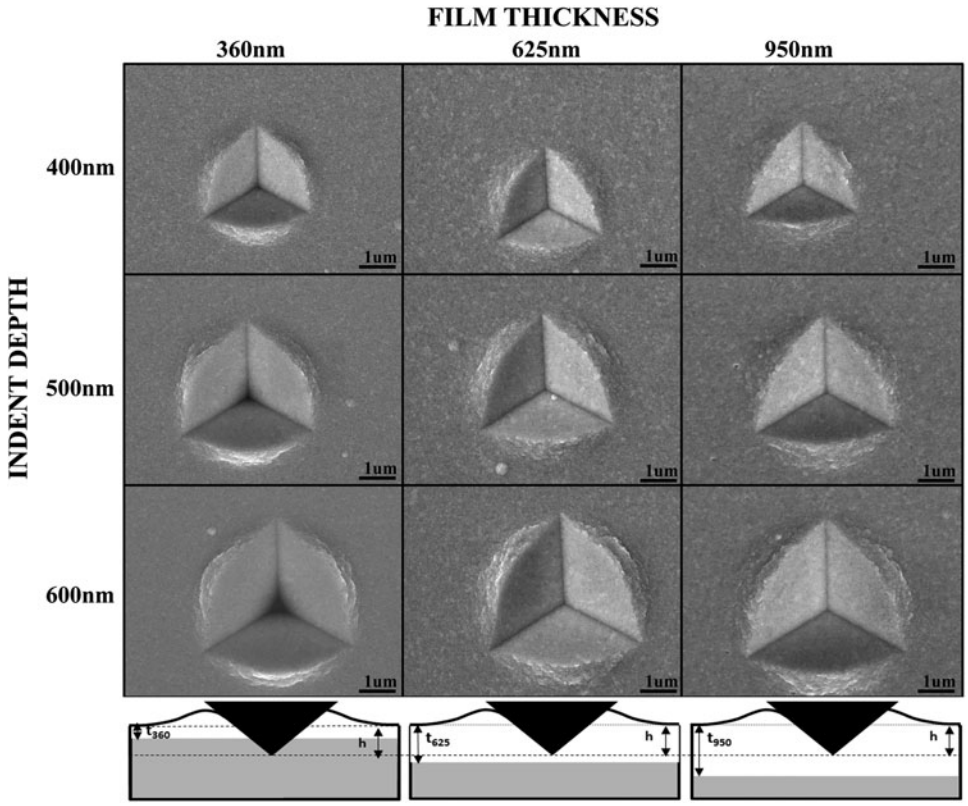


FIG. 7. Micrographs and schematics showing the same pile-up across gold on silicon at the same indent depths for different film thicknesses. Schematics below each column show the cross-section of an indent at 600 nm indent depth.

https://doi.org/10.1557/jmr.2015.167 Published online by Cambridge University Press

ImageJ software. Here, the micrograph is imported into ImageJ and then the features of the indent are traced, seen in Fig. 4. First, the projected area from only the indenter is traced by the three corners of the Berkovich tip, denoted by the dashed line in Fig. 4(b). Next, the outer boundary of the total indent contact area is traced, denoted by the solid line in Fig. 4(b). It was realized that there may be some subjectivity in this method, but the authors verified that results did not vary when performed by several separate individuals. Future work will focus on standardizing this method further. The ImageJ software then determined the area of each defined shape by counting pixels. The difference between the two measurements was the projected contact area of only the piled-up region.

An example of this analysis for the 360 nm gold film on silicon is shown in Fig. 5. Here, a series of 9 indents were created to depths ranging from 200 to 600 nm. The measured projected contact area from the Berkovich tip only is denoted by the open triangles (△) and is verified as an accurate measurement by comparing it with the Berkovich tip's calculated contact area using: $A = 24.5h_c^2$ (dashed line). The open squares (□) indicate the measured total projected contact area, and their difference is the projected pile-up area, closed circles (●). All three trends increase as expected with indent depth. The vertical solid line shows the point at which the indenter penetrated through the 360 nm thick film. Interestingly, even past the film thickness, the pile-up trends still hold. It should be noted that at indent depths below 200 nm, there was not sufficient pile-up to use this technique.

The projected contact area was also measured for the other two gold films on silicon, 625 and 950 nm, and compared with the 360 nm gold film in Fig. 6. Here, only the projected pile-up area is plotted versus indenter displacement into the surface, and error bars are shown as the average of four measured indent pile-up areas at each depth. The data from all three film thicknesses align and exhibit the same behavior. In other words, as the indenter penetrated into each film, the degree of pile-up developed was independent of film thickness. Considering that these three film/substrate combinations represented three different composite forms, an indent of a specific depth in all three would engage the substrate in different amounts. The results in Fig. 6 then suggest that the degree of pile-up was not influenced by the film thickness. It appeared to be solely dependent on the indent depth.

Further verification of this finding is seen when comparing residual indents at the same depth for different film thicknesses, seen in Fig. 7. Here, each row represents a single indent depth, whereas each column represents a particular film thickness. All micrographs were taken at

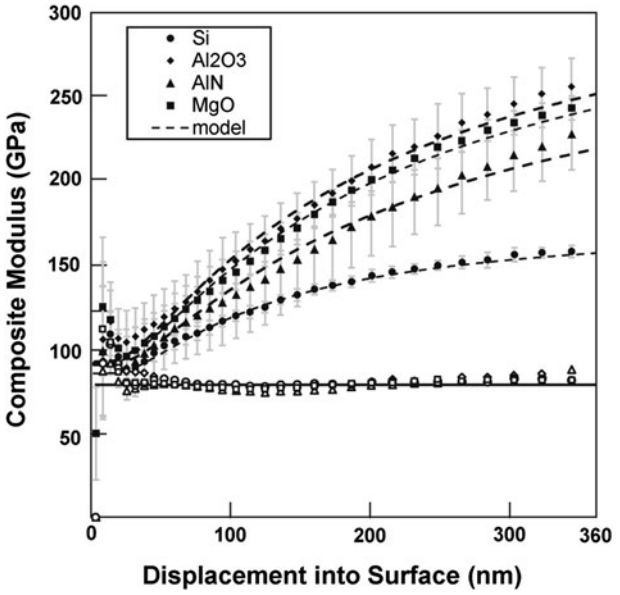


FIG. 8. Experimental data of composite modulus versus displacement into surface for 360 nm gold films deposited on substrates Si, Al_2O_3, AlN, and MgO (closed markers). All follow the Zhou–Prorok model (dashed lines) and predict a constant film modulus (open markers).

TABLE III. Film and substrate properties used in the Zhou–Prorok model.

Material	Substrate elastic modulus, E (GPa)	Substrate Poisson's ratio, ν	Film elastic modulus, E (GPa)	Film Poisson's ratio, ν	Film thickness (nm)
Si	179	0.27	79	0.44	360
Al_2O_3	350	0.22	79	0.44	360
AlN	316	0.26	79	0.44	360
MgO	345	0.23	79	0.44	360

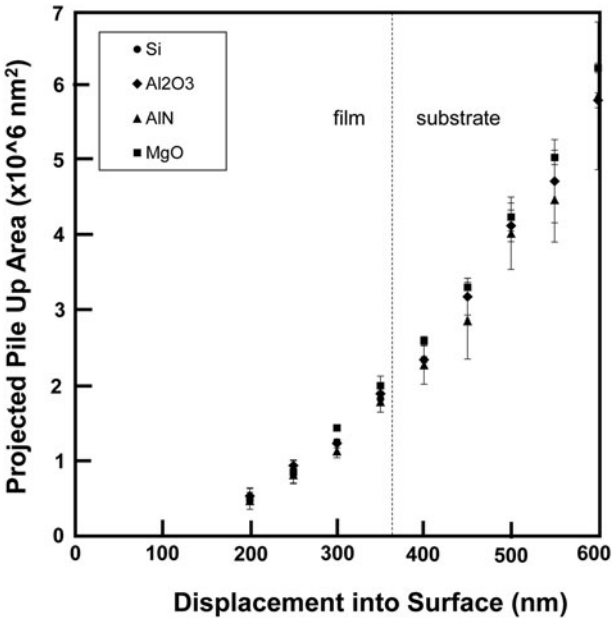


FIG. 9. Projected pile-up area versus displacement into surface for all 360 nm thick gold films on substrates, following the same trend, even past penetrating past the film thickness.

https://doi.org/10.1557/jmr.2015.167 Published online by Cambridge University Press

the same magnification. In accordance with the ImageJ results, the pile-up appears to be visually equivalent between the three films when indented to the same depth. Below each column in Fig. 7, there is a schematic illustrating the cross-section of each indent for the 600 nm indent depth. Here, each film (white) on silicon substrate (gray) is depicted with an indent approximately 600 nm deep (h), into each film. For the 360 nm film, the indent has significantly penetrated to the substrate while the indenter remains in the film for the two thicker samples. Using a conventional concept of indenting a film/substrate composite and considering the wide difference in composite moduli measured in Fig. 2(a), one would expect these three indents to appear significantly different. However, the degree of pile-up does not appear to be influenced by the film thickness or the presence of the substrate at all. It begs to question then if the degree of pile-up, being insensitive to film thickness, is also insensitive to substrate elastic modulus.

To assess whether the degree of plastic pile-up was insensitive to the substrate elastic modulus, gold films were also simultaneously deposited on Si, Al_2O_3, AlN, and MgO substrates and then subsequently indented. For the 360 nm thick gold film, composite modulus was plotted as a function of displacement into the surface in Fig. 8. Here, the film/substrate composites with the stiffer substrate yielded higher composite modulus values, as expected. In these cases, the Zhou–Prorok model continued to adeptly predict the average behavior for each film/substrate combination, using values in Table I. It also extracted the film modulus for each data point (open symbols). The physical material properties used in the Zhou–Prorok model are seen in Table III, and match the ranges listed in Table I. SEM micrographs were obtained for indents in each film/substrate combination with a final indent depth increasing from 200 to 600 nm. These were analyzed via the same SEM/ImageJ method with projected pile-up area plotted in Fig. 9. Much like the varying film thickness results from Fig. 6, the projected pile-up area followed the same trend and appeared insensitive to the substrate's modulus. Also noteworthy is that after penetrating the film (400 nm and deeper) the pile-up continues to develop in the same manner, further suggesting insensitivity to the presence of the substrate. Figure 10 shows the indent micrographs at 400 nm depth for visual confirmation, suggesting that the degree of pile-up was insensitive to the substrate's elastic properties.

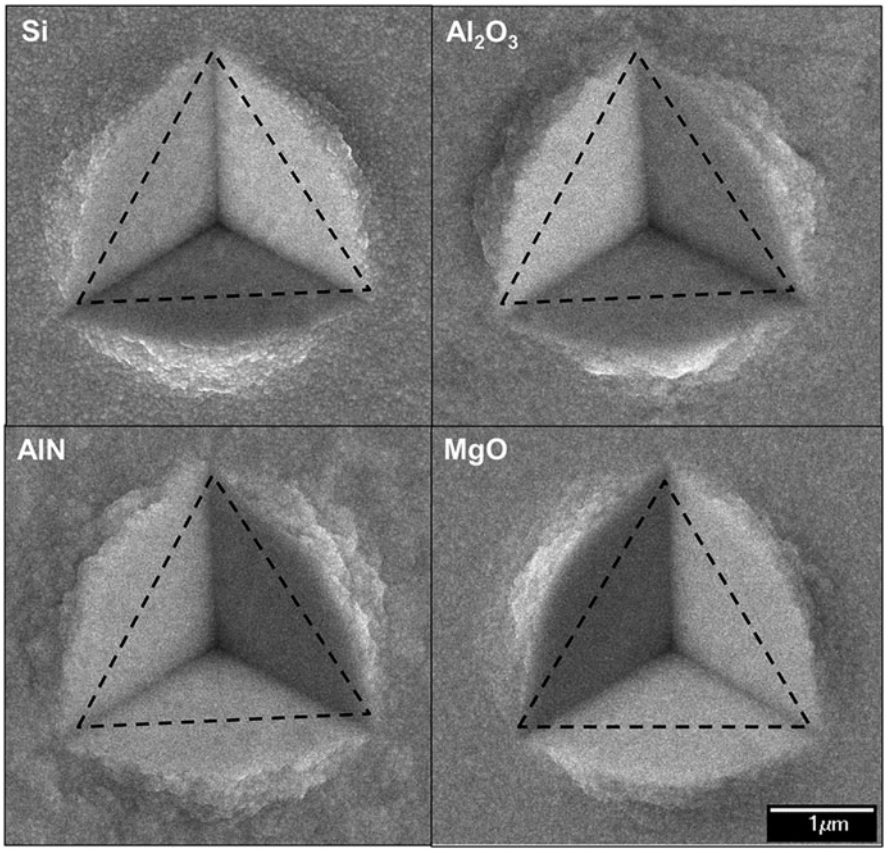


FIG. 10. Micrographs at the same magnification for Si, Al_2O_3, AlN, and MgO. Dashed triangles are identical and represent the projected area from the Berkovich tip.

https://doi.org/10.1557/jmr.2015.167 Published online by Cambridge University Press

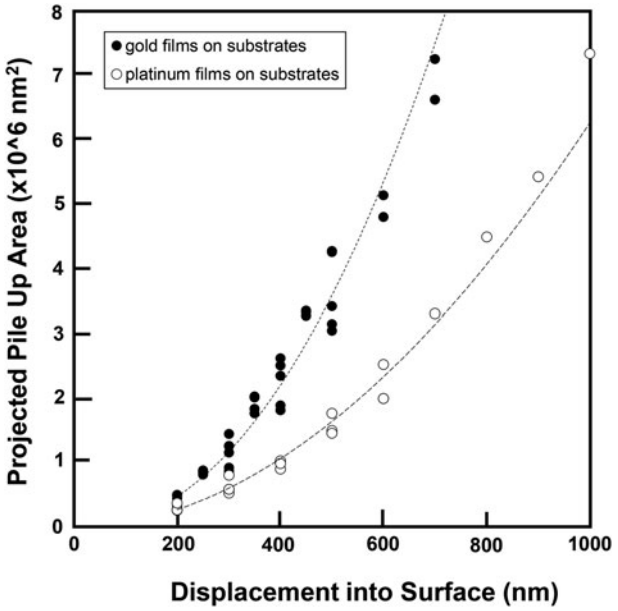


FIG. 11. Projected pile-up area plotted against displacement into surface for gold data presented thus far (●) and platinum of different thicknesses on silicon (○).

The analysis was repeated using platinum films to confirm the gold results. Figure 11 plots the measured projected pile-up area for platinum films of four different thicknesses (○) as well as all the gold film data presented thus far (●). As with gold, platinum film pile-up was not influenced by film thickness or presence of the substrate. The plot indicates that at any particular indent depth, the gold film experienced more pile-up than the platinum. Although both films are more compliant than the substrate, the gold film was significantly more compliant. However, these pile-up differences cannot be linked to the film elastic moduli. It was established that the Zhou–Prorok model accurately modeled and predicted the elastic behavior of the composite based upon the contribution of the individual components. This model was also found to not be influenced by the degree of pile-up. Thus, the difference then is more likely to be related to the onset of plastic deformation in these materials. This method and its results may segue to eventually enabling the extraction of plastic properties from minimally invasive indentation.

IV. CONCLUSIONS

These results indicated that when indenting the specific system of a metallic compliant, plastically deforming film on a stiff, nonplastically deforming ceramic-like material, the additional indenter-film contact that occurs from pile-up did not influence the elastic unloading process. The pile-up was independent of film thickness and the elastic properties of the substrate. These findings appear to counter the generally accepted understanding that the additional contact due to pile-up influences the extraction of elastic properties from the indents. The results indicated that corrections to the contact area are not necessary when extracting film modulus from the composite experimental data. These findings will aid researchers in more reliably extracting elastic properties of thin films.

REFERENCES

1. W.C. Oliver and G.M. Pharr: An improved technique for determining hardness and elastic modulus using load and displacement sensing indentation experiments. *J. Mater. Res.* **7**, 1564 (1992).
2. W.C. Oliver and G.M. Pharr: Measurement of hardness and elastic modulus by instrumented indentation: Advances in understanding and refinements to methodology. *J. Mater. Res.* **19**, 3 (2004).
3. X. Li and B. Bhushan: A review of nanoindentation continuous stiffness measurement technique and its applications. *Mater. Charact.* **48**, 11 (2002).
4. M.F. Doerner and W.D. Nix: A method for interpreting the data from depth-sensing indentation instruments. *J. Mater. Res.* **1**, 601 (1986).
5. R.B. King: Elastic analysis of some punch problems for a layered medium. *Int. J. Solids Struct.* **23**, 1657 (1987).
6. R. Saha and W.D. Nix: Effects of the substrate on the determination of thin film mechanical properties by nanoindentation. *Acta Mater.* **50**, 23 (2002).
7. H. Gao, C-H. Chiu, and J. Lee: Elastic contact versus indentation modeling of multi-layered materials. *Int. J. Solids Struct.* **29**, 2471 (1992).
8. J. Hay and B. Crawford: Measuring substrate-independent modulus of thin films. *J. Mater. Res.* **26**, 727 (2011).
9. G.M. Pharr: Measurement of mechanical properties by ultra-low load indentation. *Mater. Sci. Eng., A* **253**, 151 (1998).
10. B. Zhou and B. Prorok: A discontinuous elastic interface transfer model of thin film nanoindentation. *Exp. Mech.* **50**, 793 (2010).
11. B. Zhou and B.C. Prorok: A new paradigm in thin film nanoindentation. *J. Mater. Res.* **25**, 1671–1678 (2010).
12. W.D. Nix: Elastic and plastic properties of thin films on substrates: Nanoindentation techniques. *Mater. Sci. Eng., A* **234–236**, 37–44 (1997).
13. X. Chen and J.J. Vlassak: Numerical study of the measurement of thin film mechanical properties by means of nanoindentation. *J. Mater. Res.* **16**, 2974–2982 (2001).
14. K.W. McElhaney, J.J. Vlassak, and W.D. Nix: Determination of indenter tip geometry and indentation contact area for depth-sensing indentation experiments. *J. Mater. Res.* **13**, 1300–1306 (1998).
15. A. Bolshakov and G.M. Pharr: Influences of pileup on the measurement of mechanical properties by load and depth sensing indentation techniques. *J. Mater. Res.* **13**, 1049–1058 (1998).
16. B. Taljat and G.M. Pharr: Development of pile-up during spherical indentation of elastic–plastic solids. *Int. J. Solids Struct.* **41**, 3891–3904 (2004).
17. W.D. Callister, Jr. and D.G. Rethwisch: *Fundamentals of Materials Science and Engineering: An Integrated Approach*, Vol. **3**. (John Wiley & Sons, Hoboken, NJ, 2008).
18. P. Boch, J.C. Glandus, J. Jarrige, J.P. Lecompte, and J. Mexmain: Sintering, oxidation and mechanical properties of hot pressed aluminum nitride. *Ceram. Int.* **8**, 34–40 (1982).
19. R.R. Gupta and M.D. Lechner: *Landolt-Bonstein-Group III Condensed Matter* (Springer, New York, 2005).

https://doi.org/10.1557/jmr.2015.167 Published online by Cambridge University Press

20. C. Liang and B.C. Prorok: Measuring the thin film elastic modulus with a magnetostrictive sensor. *J. Micromech. Microeng.* **17**, 709 (2007).
21. L. Wang, C. Liang, and B.C. Prorok: A comparison of testing methods in assessing the elastic properties of sputter-deposited gold films. *Thin Solid Films* **515**, 7911 (2007).
22. L. Wang and B.C. Prorok: Characterization of the strain rate dependent behavior of nanocrystalline gold films. *J. Mater. Res.* **23**, 55 (2008).
23. L. Wang and B.C. Prorok: Inverstigation of the influence of grain size, texture, and orientation on the mechanical behavior of free-standing polycrystalline gold films. *MRS Proc.* **924**, Z03–13 (2006).
24. C.A. Schneider, W.S. Rasband, and K.W. Eliceiri: NIH image to ImageJ: 25 years of image analysis. *Nat. Methods* **9**, 671 (2012).
25. H.D. Espinosa and B.C. Prorok: Size effects on the mechanical behavior of gold thin films. *J. Mater. Sci.* **38**, 4125 (2003).
26. H.D. Espinosa, B.C. Prorok, and M. Fischer: A methodology for determining mechanical properties of freestanding thin films and MEMS materials. *J. Mech. Phys. Solids* **51**, 47 (2003).
27. H.D. Espinosa, B.C. Prorok, and B. Peng: Plasticity size effects in free-standing submicron polycrystalline FCC films subjected to pure tension. *J. Mech. Phys. Solids* **52**, 667 (2004).
28. B.C. Prorok and H.D. Espinosa: Effects of nanometer-thick passivation layers on the mechanical response of thin gold films. *J. Nanosci. Nanotechnol.* **2**, 427 (2002).
29. K. Kese and Z.C. Li: Semi-ellipse method for accounting for the pile-up contact area during nanoindentation with the Berkovich indenter. *Scr. Mater.* **55**, 699 (2006).
30. K.O. Kese, Z.C. Li, and B. Bergman: Method to account for true contact area in soda-lime glass during nanoindentation with the Berkovich tip. *Mater. Sci. Eng., A* **404**, 1 (2005).
31. T.Y. Tsui, W.C. Oliver, and G.M. Pharr: Influences of stress on the measurement of mechanical properties using nanoindentation: Part I. Experimental studies in an aluminum alloy. *J. Mater. Res.* **11**, 752 (1996).
32. A. Bolshakov, W.C. Oliver, and G.M. Pharr: Influences of stress on the measurement of mechanical properties using nanoindentation: Part II. Finite element simulations. *J. Mater. Res.* **11**, 760 (1996).

https://doi.org/10.1557/jmr.2015.167 Published online by Cambridge University Press